Available online at www.sciencedirect.com
ScienceDirect
Trans. Nonferrous Met. Soc. China 27(2017) 747−753
Transactions of Nonferrous Metals Society of China
www.tnmsc.cn

Microstructure evolution during homogenization of Al−Mg−Si−Mn−Fe alloys: Modelling and experimental results

C. L. LIU[1], H. AZIZI-ALIZAMINI[2], N. C. PARSON[3], W. J. POOLE[1], Q. DU[4]

1. Department of Materials Engineering, The University of British Columbia, Vancouver V6T 1Z4, Canada;
2. Department of Materials Science and Engineering, McMaster University, Hamilton L8S 4L7, Canada;
3. Rio Tinto, Arvida Research and Development Centre, P. O. Box 1250, Jonquière (QC) G7S 4K8, Canada;
4. SINTEF Materials and Chemistry, P. O. Box 4760 Sluppen, 7456 Trondheim, Norway

Received 3 May 2016; accepted 8 December 2016

Abstract: Microstructure evolution during the homogenization heat treatment of an Al−Mg−Si−Fe−Mn (AA6xxx) alloy was investigated using a combination of modelling and experimental studies. The model is based on the CALPHAD-coupled homogenization heat treatment model originally developed for AA3xxx alloys (i.e., Al−Mn−Fe−Si). In this work, the model was adapted to the more complex AA6xxx system (Al−Mg−Si−Mn−Fe) to predict the evolution of critical microstructural features such as the spatial distribution of solute, the type and fraction of constituent particles and dispersoid number density and size distribution. Experiments were also conducted using three direct chill (DC) cast AA6xxx alloys with different Mn levels subjected to various homogenization treatments. The resulting microstructures were characterized using a range of techniques including scanning electron microscopy, electron microprobe analysis (EPMA), XRD, and electrical resistivity measurements. The model predictions were compared with the experimental measurements, and reasonable agreement was found.
Key words: AA6xxx alloy; homogenization heat treatment; mathematical modelling; CALPHAD; diffusion

1 Introduction

The aluminum alloy, AA6082, is commonly used as extrusion alloy due to its good combination of formability and corrosion resistance. Billets are mainly produced by direct chill (DC) casting and may have a range of Mn and Fe contents. The non-equilibrium nature of solidification (i.e., relatively high cooling rates and growth velocities) leads to micro-segregation and formation of a wide range of intermetallic phases [1]. These ingots have to undergo a homogenization treatment before extrusion to eliminate micro-segregation, modify the intermetallic phase type and morphology to improve extrudability [2]. It is apparent that microstructure changes such as the transformation of large constituent particles, the formation of dispersoids and the precipitation/dissolution of precipitates during homogenization influence the downstream extrusion behavior and the subsequent microstructure development [3−5]. The development of microstructure and the effect on final properties are influenced by both alloy additions and heat treatment parameters [6].

In 6xxx alloys, α-Al(MnFe)Si, β-AlFeSi and Mg_2Si constituent particles form during solidification [7,8], and can be characterized using EDX and EBSD in the as-cast condition [9]. The first phase to form is α-Al(MnFe)Si which may or may not contain Mn or Fe depending on the chemistry. COOPER et al [10,11] examined the crystal structure of this α-Al(MnFe)Si phase in the Al−Mn−Si system where this phase was found to have a simple cubic structure [10]. However, the phase changes to a BCC structure when Fe replaces Mn [11]. In contrast, the β-AlFeSi phase has sharp boundaries and is poorly bonded with the Al matrix which leads to poor hot workability [12]. A transition from plate like β-AlFeSi phase to a more spheroidized α-Al(FeMn)Si phase has been reported after homogenization [13]. It is believed that the presence of the α-Al(FeMn)Si phase improves surface finish and extrudability [14]. ZAJAC et al [14] found that Al−Mg−Si alloys alloyed with Mn greatly accelerate this transformation during homogenization. The transformation mechanism from β-AlFeSi phase to spheroidized α-Al(FeMn)Si phase was proposed to

Corresponding author: W. J. POOLE; E-mail: warren.poole@ubc.ca
DOI: 10.1016/S1003-6326(17)60085-2

initiate with the nucleation of the α phase on top or side of the β phase during homogenization [15,16]. Finally, the Mg_2Si phase dissolves very quickly when the alloy is held above its solvus temperature dependent on the composition [17], but may act as nucleation sites for dispersoids during the ramp heating to the homogenization temperature [18].

Turning to the dispersoid phase, DOWLING and MARTIN [6] studied two Fe-free Mn-bearing 6xxx alloys with different Mn contents and found that the dispersoids are incoherent α-$Al_{12}Mn_3Si$ particles. In the case of Fe-containing alloys, the crystal structure of these dispersoids depends on the mole ratio of Mn/Fe [6,19], i.e., simple cubic structure is found for higher Mn/Fe mole ratios while a lower Mn/Fe mole ratio favors the BCC structure. LODGAARD and RYUM [18] studied the sequence of precipitation in Al−Mg−Si alloys with different Mn contents. They found that α-Al(MnFe)Si dispersoids heterogeneously nucleate on "*u*-phase" which is an intermediate or transition phase precipitate of Mg_2Si during heating to the homogenization temperature.

The above observations indicate that the transformation of primary constituent particles (particles of 0.5−5 μm) and the formation of dispersoids (20−200 nm) are both affected by the alloying and homogenization scenarios. Thus, it would be desirable to have a chemistry dependent homogenization model predicting the evolution of these particles. Such a model was reported by DU et al in Ref. [20] where a CALPHAD-coupled homogenization model was developed and validated for AA3xxx (Al−Mn−Fe−Si alloys). The current study is an extension of the model to the more complex AA6xxx (Al−Mg−Si−Mn−Fe) alloys. Our aim is to examine the predictive power of the model for the design of 6xxx alloys and heat treatment parameters using a detailed comparison to experimental measurements.

2 Model description

The multi-scale homogenization model which has been adapted to the current study was previously described in Ref. [20] and as such only a brief summary is given below. It consists of a macroscopic 1D solute diffusion equation for the growth of constituent particles and their transformation and a microscopic based model to describe dispersoid nucleation and growth. The finite volume method described in Ref. [21] is employed to solve the diffusion equation at the scale of the dendrite arm spacing:

$$\frac{\partial x_i^m}{\partial t} = \nabla \cdot (D_i \nabla x_i^m) \quad (1)$$

where x_i^m is the solid solution level of solute i, and D_i is the diffusion coefficient of the diffusion species including Mg, Si, Mn and Fe. An interface cell always separates the matrix and the inter-granular mixture cell.

The microscopic model is the KWN model described in Ref. [22]. It is applied to each volume element of the 1D domain to capture the precipitation kinetics resulting from the variation in local chemistry. The main assumptions adopted in the extended model are as follows.

1) Mn-bearing dispersoids are of spherical shape and their growth/dissolution is solely controlled by diffusion. Mg_2Si particles are not considered, i.e., they are assumed to dissolve at homogenization temperatures of interest.

2) Local equilibrium modified by the Gibbs−Thomson effect prevails at the precipitate−matrix interface and in interdendritic regions.

3) The diffusion field surrounding each dispersoid is at quasi-steady state.

These two models are tightly coupled and involve two length scales. The splitting method adopted in Ref. [20] was employed in this work to deal with the coupling. Readers are referred to Ref. [20] and the references therein for the complete details. The model is also extended to study the effect of Cr on homogenization in AA3xxx alloys [23].

The input parameters for the model are the alloy composition, the thermal history, the phase diagram (thermodynamic database Thermocalc 4.1 with TTAL6), thermo-physical parameters such as diffusivities and the interfacial energy and the number density of nucleation sites. The model can then predict the evolution of dispersoids free zone (DFZ), constituent particle type and fraction, solid solution solute levels and size distribution of dispersoids. The diffusivity of the alloying species (Mn, Fe, Si and Mg) was taken from the work of DU et al [24]. The interfacial energy used in the simulation is 0.08 J/m^2. After several runs of fitting, the number of heterogeneous nucleation sites was chosen as 2.5×10^{19} m^{-3}. The secondary dendrite arm spacing is about 20 μm based on measurements in various as-cast samples with different Mn contents.

3 Experimental

3.1 Materials and heat treatment

Three as-cast Al−Mg−Si alloys were prepared as billets with 100 mm in diameter and 300 mm in length by the Rio Tinto Aluminum Research and Development Center (ARDC) in Jonquiere, Quebec. The chemical compositions of these alloys are listed in Table 1. The chemical compositions for alloys 1, 2 and 3 are designed to investigate the effect of Mn on microstructure changes

during homogenization.

Homogenization for the as-cast samples was conducted using a Carbolite™ (HRF) recirculating air furnace. A separate thermocouple welded on a dummy sample was used to monitor the temperature and to record the thermocouple data via instuNet^{TM} software and instruNet Model 100 DAQ system. The ramping rate was 200 °C/h for all the samples. The soaking time at specific target temperatures of 550 and 580 °C (above the solvus temperature of Mg_2Si calculated by Thermo Calc (TTAL6 database) varied from 0 to 168 h. After soaking, the samples were water-quenched.

Table 1 Chemical compositions of different Al−Mg−Si alloys (mass fraction, %)

Alloy No.	Designation	Mg	Si	Mn	Fe	Al
1	0Mn	0.71	0.91	0.003	0.20	Bal.
2	0.25Mn	0.71	0.95	0.25	0.21	Bal.
3	0.5Mn	0.71	1.03	0.50	0.21	Bal.

3.2 Experimental characterization techniques

Electron microprobe analysis (EPMA) was used to analyze the distribution of the main alloying elements before and after homogenization. The EPMA measurements were conducted on a fully automated CAMECA SX−50 instrument, operating in the wavelength-dispersion (WDS) mode. The samples were first cold-mounted, ground, polished and then carbon-coated for 24 h before the test. The excitation voltage was 15 kV and the beam current was 20 nA. The beam size was 1 μm and the distance chosen between two measurements was 5 μm. Random lines crossing the samples were drawn for the measurements. About 200 points were measured for each sample. Electrical resistivity measurements were conducted using a Sigmatest® 2.069 eddy current conductivity meter for the as-cast and homogenized samples. A frequency of 60 kHz was selected for all measurements. Output data are in the form of electrical conductivity in the units of MS/m which was converted into electrical resistivity in nΩ·m. A Zeiss FEG-SEM operated at 5 kV was used to characterize the dispersoids and constituent particles in the specimen. The samples were mechanically ground and polished with final step polishing using colloidal silica. The images were collected using the backscatter electron (BSE) mode where Mn-containing constituent particles and dispersoids are better revealed due to their high atomic number contrast with aluminum. High magnification images, 1000 and 20000 times, were used for constituent particles and dispersoids, respectively, in order to conduct quantitative analysis using the ImageJ® program. XRD analysis on extracted constituent particles was performed by dissolving the aluminum matrix with phenol at 180 °C. The undissolved constituent particles were scanned in the diffractometer for 2θ values of 5° to 80° using K_α X-ray. The fine-focus Co X-ray tube was operated at 35 kV and 40 mA.

4 Results and discussion

4.1 Spatial distribution of solutes

The electron probe micro analysis (EPMA) was conducted on the three AA6082-based alloys with different Mn additions. In Al−Mg−Si−Mn alloys, both Mg and Si are fast diffusion elements which are dissolved quickly in the aluminum matrix during homogenization above the Mg_2Si solvus [25]. As Fe has a very low solubility in Al, only Mn profiles are plotted from the EPMA measurements and compared with the homogenization model predictions.

Figure 1 provides a comparison of the experimental and simulation results for the 0.5Mn alloy held at 550 °C for various soaking periods. It is important to note that the data from the EPMA in Fig. 1(a) are sorted from

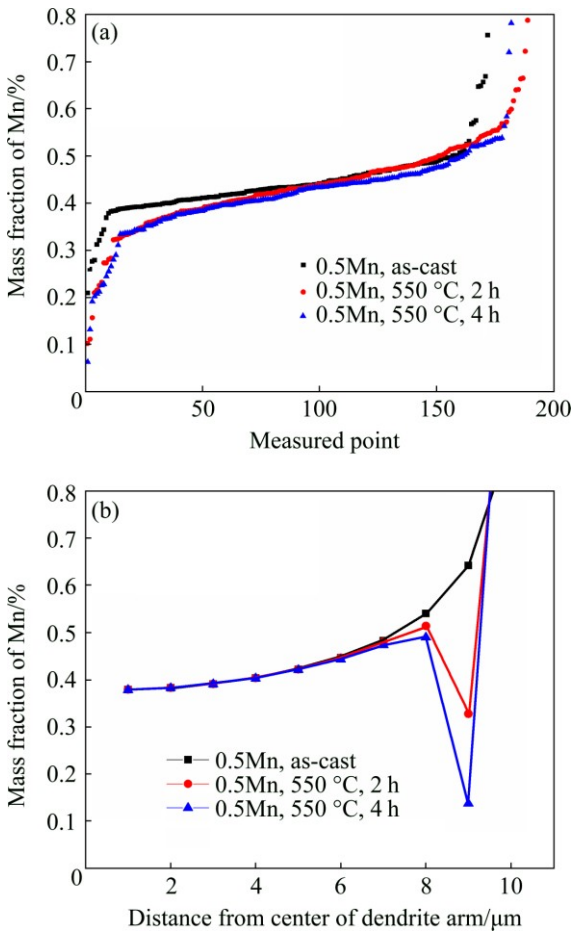

Fig. 1 Mn content profiles from different conditions in 0.5Mn alloy: (a) EPMA measurements (Mn data sorted from smallest to largest); (b) Model prediction (from dendrite center to interdendritic area)

the lowest to the highest according to GANESAN et al [26] and such spatial information is lost so one has to be careful comparing the experimental and simulation results (the sorting was done as the spatial resolution of the EPMA was insufficient to capture the variation within a single dendrite). Nevertheless, good agreement is found between Mn composition profiles from the model in Fig. 1(b) and the sorted Mn compositions measured by EPMA in Fig. 1(a), i.e., the maximum and minimum contents of Mn are in agreement. In Fig. 1(b), the black square symbols show the Mn profile from the center to the interdendritic area of a dendrite arm. As Mn is supersaturated during solidification, the highest level of Mn in solid solution was found in the 0.5Mn as-cast sample, as expected. Soaking the as-cast samples at 550 °C promotes the formation of Mn-containing dispersoids and mass transfer by the diffusion of Mn to the large constituent particles. The depletion of Mn in the matrix at the vicinity of constituent particles results in a local decrease of Mn content as can be seen in Fig. 1(b). However, the EPMA results could not resolve this local change in composition or differentiate Mn in solid solution from Mn in dispersoids because of the relatively large interaction volume (2 to 3 μm in diameter), i.e., the depletion zone is about 1 μm and the dispersoids are less than 100 nm in radius.

Further EPMA measurements and simulations were performed at a higher homogenization temperature of 580 °C for hold periods up to 12 h. In Fig. 2, the Mn content from the EPMA measurements is averaged (excluding the data which came partially from the constituent particles, i.e., for Mn contents approximately larger than 0.5%) and compared with the simulation output averaged from cell 1 to cell 9. In general, the model gives a good description of the experimental results. One discrepancy is found for the 0.5Mn alloy which is homogenized at 580 °C for 12 h. The model gives a lower Mn level compared to the experiment, which means that more Mn is predicted to be transported to the constituent particles than the experimental results of Mn from microprobe. This suggests that the kinetics of Mn long-range diffusion from the primary Al to constituent particles is overestimated by the model.

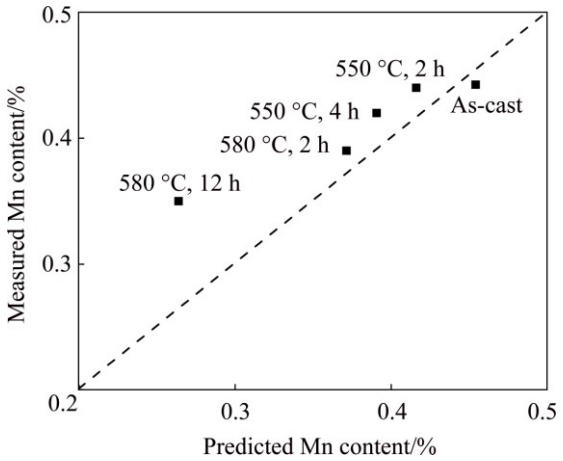

Fig. 2 Average measured and predicted Mn contents (mass fraction) in 0.5Mn alloy

4.2 Constituent particles and dispersoids

During homogenization, a transformation of the constituent particles occurs for the 0.5Mn alloy. Figure 3(a) shows the prediction for the evolution of the constituent particles. The dissolution of the Mg_2Si phase is determined by its solvus temperature and the volume fraction of β phase (β-AlFeSi) decreases while the α phase (α-Al(MnFe)Si) increases, i.e., β-AlFeSi is transformed into α-Al(MnFe)Si during homogenization. The transformation is complete at the end of the heating ramp leaving only α phase in the microstructure for the rest of the soak period. Figure 3(b) shows the results from EPMA studies, indicating that the (Fe+Mn)/Si mole ratio remains constant at all time and temperatures greater than 10 min and 550 °C, respectively. This ratio

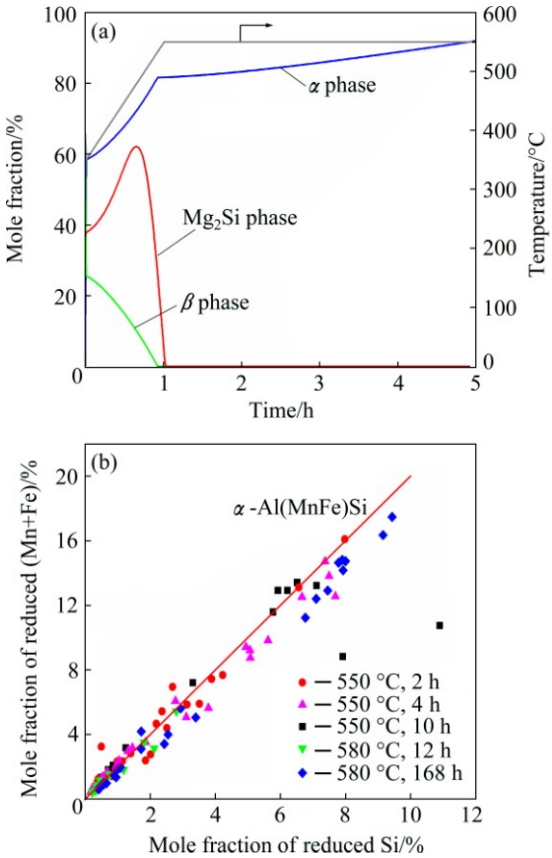

Fig. 3 Constituent particles evolution in 0.5Mn alloy homogenized at 550 °C: (a) Modeling prediction for constituent phases; (b) Mole fraction of reduced (Fe+Mn) vs reduced Si content from EPMA or partially from constituent particles (Note: the reduced Mn and Si levels have been obtained by subtracting the matrix background levels from overall measurement)

is consistent with the constituent particles being the α-Al(MnFe)Si type phase, i.e., consistent with the model predictions.

Figure 4(a) shows the typical morphology of constituent particles for the 0.5Mn alloy homogenized at 550 °C for 2 h. When examined at higher magnification, one can also observe the Mn-bearing dispersoids as shown in Fig. 4(b). These dispersoids play an important role in controlling the grain structure during high temperature deformation and also increase the high temperature flow stress. The mean equivalent radius from the experiments is 43 nm and the model gives a mean radius of 44 nm, showing a good match in terms of dispersoid mean radius.

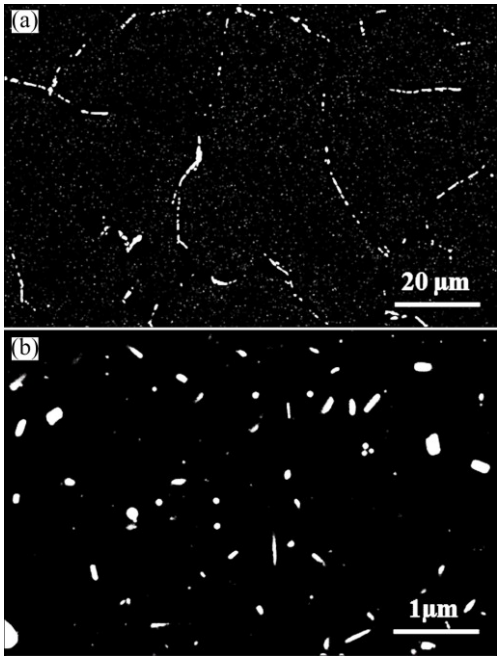

Fig. 4 Constituent particles and dispersoids in 0.5Mn alloy homogenized at 550 °C for 2 h: (a) Lower magnification BSE image showing constituent particles; (b) Higher magnification BSE image showing Mn-bearing dispersoids

4.3 Alloy with low Mn content

Further experimental and modeling work was conducted on the 0.25Mn alloy. It was found that the model could also describe the constituent particles transformation from β-AlFeSi type to α-Al(MnFe)Si type in this case. The difference compared with the 0.5Mn alloy is that the kinetics of the transformation is much slower. The model predicts that for the case of the low Mn level, it will take soaking time of approximately 4 h at 550 °C to fully transform β-AlFeSi to α-Al(MnFe)Si phase. This is validated by the experiment from EPMA shown in Fig. 5(b) where it can be seen that the β-AlFeSi and α-Al(MnFe)Si phases coexist in the sample homogenized at 550 °C for 2 h or less. However, when soaking time is increased to 4 h, the (Fe+Mn)/Si mole ratio is consistent with only α-Al(MnFe)Si constituent particles being present.

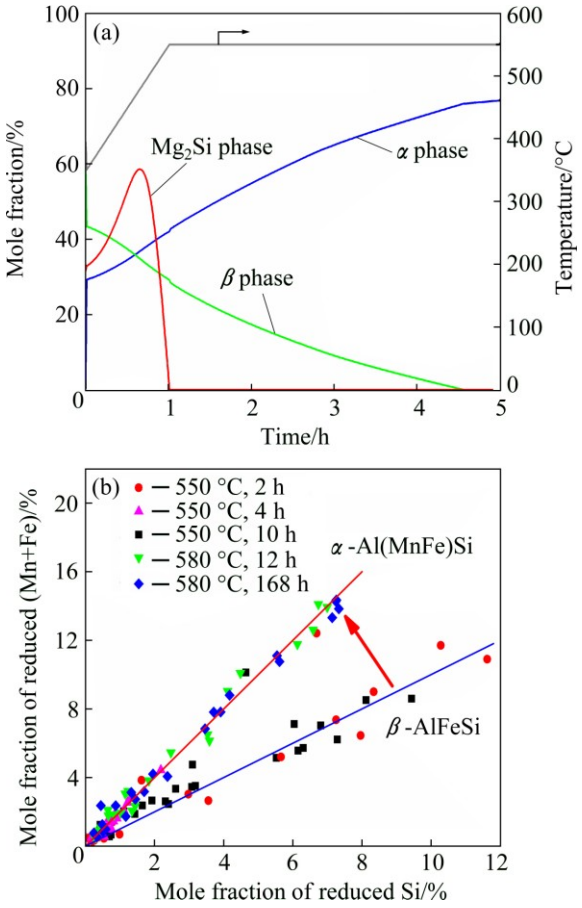

Fig. 5 Constituent particles evolution in 0.25Mn alloy homogenized at 550 °C: (a) Modeling prediction for constituent phases; (b) Reduced (Fe+Mn) content vs reduced Si content from EPMA or partially from constituent particles (Note: the reduced Mn and Si levels have been obtained by subtracting the matrix background levels from overall measurement)

In order to quantify the amount of α and β type constituent particles, the aluminum matrix was dissolved and the constituent particles were collected. From Fig. 5(a), the mass fractions of α-Al(MnFe)Si phase at 550 °C for 2 h and 550 °C for 4 h are 88% and 100%, respectively. Correspondingly, the quantitative results from the XRD analysis (using a Rietveld analysis) on the extracted constituent particles give 83% and 96% for α-Al(MnFe)Si phase for the two different soaking time of 2 and 4 h, respectively. The solid solution levels predicted from the model can also be compared with the experimental electrical resistivity measurements by converting the model solid solution levels in the matrix to resistivity using Matthiessen's law as shown in Fig. 6. The resistivitys of Mn, Fe, Si and Mg were taken as 29.4, 25.6, 6.2 and 5.4 nΩ·m from HATCH [2], except the value for Si was corrected from LOK [27]. Both the model predicted and experimental measurements show

an initial drop to a local minimum value at the temperature of 500 °C and then rise to a local maximum (at around 550 °C). The simulation reveals that the initial drop is due to the decrease of Mg and Si solid solution levels. From the model output, the Mg_2Si constituents only dissolve when the temperature is above 550 °C. After reaching the maximum, the resistivity drops as the Mn content in solid solution decreases due to precipitation of dispersoids. In the future, it will be interesting to take into account the Mg_2Si precipitation kinetics for better predictions during the temperature ramp to the homogenization temperature.

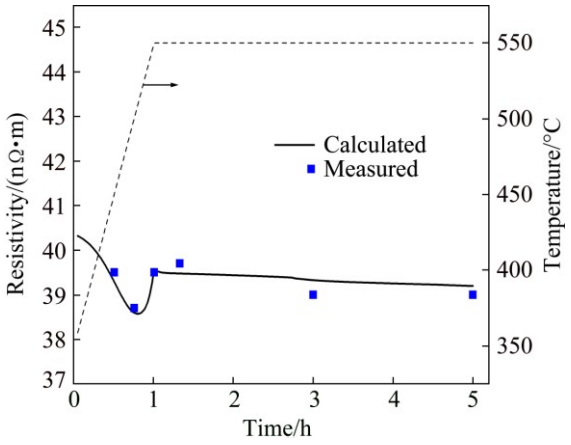

Fig. 6 Predicted resistivity evolution from model and measured resistivity in 0.25Mn alloy

However, a discrepancy was found for the 0.25Mn alloy when comparing the dispersoid mean size between the model and the corresponding FEG-SEM characterization. The experimental result gives a mean radius of 45 nm, almost the same as that in 0.5Mn alloy, suggesting that the Mn content has little effect on dispersoid size. However, the model predicts a mean radius of 30 nm which is considerably different from the experimental observation. This may be related to the change in nucleation mechanism for different supersaturation levels and is currently under further investigation.

5 Conclusions and future work

1) The chemistry dependent homogenization model developed for AA3xxx alloys was adopted to examine microstructure evolution during homogenization of AA6xxx alloys which contain Fe and Mn. A series of characterization techniques were employed to validate the model.

2) It was found that the model could capture the major microstructure feature such as the Mn composition profiles and the type of constituent particles.

3) The dispersoid size and solid solution levels could also be predicted with good agreement found for the 0.5Mn alloy, but not for the 0.25Mn alloy.

4) In addition to this issue, there is some room for further improvement. The transformation of β-AlFeSi to α-Al(MnFe)Si constituent particles is not taken into account during casting or during the cooling stage before homogenization and neither is Mg_2Si formation and dissolution during ramping. The model's predictive power can be improved if the two processes are incorporated into the model in the future.

Acknowledgements

Financial support from Rio Tinto Aluminium and NSERC are gratefully acknowledged.

References

[1] NADELLA R, ESKIN D G, DU Q, KATGERMAN L. Macrosegregation in direct-chill casting of aluminium alloys [J]. Progress in Materials Science, 2008, 53: 421−480.

[2] HATCH J E. Aluminium: Properties and physical metallurgy [M]. Ohio: ASM International, 1984.

[3] BIROL Y. Homogenization of EN AW 6005A alloy for improved extrudability [J]. Metallurgical and Materials Transactions A, 2013, 44: 504−511.

[4] DONS A L. The Alstruc homogenization model for industrial aluminum alloys [J]. Journal of Light Metals, 2001, 1: 133−149.

[5] PARSON N C, YIU H L. The effect of heat-treatment on the microstructure and properties of 6000 series alloy extrusion ingots [C]//Proc Light Metals 1989. Phoenix, AZ: TMS, 1988: 713−724.

[6] DOWLING J M, MARTIN J W. Influence of Mn additions on deformation-behavior of an Al−Mg−Si alloy [J]. Acta Metallurgica, 1976, 24: 1147−1153.

[7] HSU C, O'REILLY K, CANTOR B, HAMERTON R. Non-equilibrium reactions in 6xxx series Al alloys [J]. Materials Science and Engineering A, 2001, 304−306: 119−124.

[8] SHA G, O'REILLY K, CANTOR B, WORTH J, HAMERTON R. Growth related metastable phase selection in a 6xxx series wrought Al alloy [J]. Materials Science and Engineering A, 2001, 304−306: 612−616.

[9] SWEET L, ZHU S, CAO S, J. TAYLOR J, EASTON M. The Effect of Iron content on the Iron-containing intermetallic phases in a cast 6060 aluminum alloy [J]. Metallurgical and Materials Transactions A, 2011, 42: 1737−1749.

[10] COOPER M, ROBINSON K. The crystal structure of the ternary alloy α(AlMnSi) [J]. Acta Crystallographica, 1966, 20: 614−617.

[11] COOPER M. The crystal structure of the ternary alloy α(AlFeSi) [J]. Acta Crystallographica, 1967, 23: 1106−1107.

[12] MULAZIMOGLU M H, ZALUSKA A, GRUZLESKI J E, PARAY F. Electron microscope study of Al−Fe−Si intermetallics in 6201 aluminum alloy [J]. Metallurgical and Materials Transactions A, 1996, 27: 929−936.

[13] KUIJPERS N C W, KOOL W H, KOENIS P T G, NILSEN K E, TODD I, van der ZWAAG S. Assessment of different techniques for quantification of α-Al(FeMn)Si and β-AlFeSi intermetallics in AA 6xxx alloys [J]. Materials Characterization, 2002, 49: 409−420.

[14] ZAJAC S, HUTCHINSON B, JOHANSSON A, GULLMAN L O. Microstructure control and extrudability of Al−Mg−Si alloys microalloyed with manganese [J]. Materials Science and Technology, 1994, 10: 323−333.

[15] KUIJPERS N C W, TIREL J, HANLON D N, van der ZWAAG S. Characterization of the α-Al(FeMn)Si nuclei on β-AlFeSi intermetallics by laser scanning confocal microscopy [J]. Journal of Materials Science Letters, 2003, 22: 1385−1387.
[16] KUIJPERS N C W, VERMOLEN F J, VUIK K, van der ZWAAG S. A model of the β-AlFeSi to α-Al(FeMn)Si transformation in Al−Mg−Si alloys [J]. Materials Transactions, 2003, 44: 1448−1456.
[17] PRIYA P, KRANE M J M, JOHNSON D R. A numerical and experimental study of homogenization of Al−Si−Mg alloys [C]//Proc Light Metals 2014. San Diego, CA: TMS, 2014: 423−428.
[18] LODGAARD L, RYUM N. Precipitation of dispersoids containing Mn and/or Cr in Al−Mg−Si alloys [J]. Materials Science and Engineering A, 2000, 283: 144−152.
[19] YOO J E, SHAN A, MOON I G, MAENG S J. A study on composition and crystal structure of dispersoids in AlMgSi alloys [J]. Journal of Materials Science, 1999, 34: 2679−2683.
[20] DU Q, POOLE W J, WELLS M A, PARSON N C. Microstructure evolution during homogenization of Al−Mn−Fe−Si alloys: Modeling and experimental results [J]. Acta Materialia, 2013, 61: 4961−4973.
[21] DU Q, JACOT A. A two-dimensional microsegregation model for the description of microstructure formation during solidification in multicomponent alloys: Formulation and behaviour of the model [J]. Acta Materialia, 2005, 53: 3479−3493.
[22] DU Q, POOLE W J, WELLS M A. A mathematical model coupled to CALPHAD to predict precipitation kinetics for multicomponent aluminum alloys [J]. Acta Materialia, 2012, 60: 3830−3839.
[23] DU Q, LI Y J. Effect modeling of Cr and Zn on microstructure evolution during homogenization heat treatment of AA3xxx alloys [J]. Transactions of Nonferrous Metals Society of China, 2014, 24: 2145−2149.
[24] DU Y, CHANG Y A, HUANG B, GONG W, JIN Z. Diffusion coefficients of some solutes in fcc and liquid Al: Critical evaluation and correlation [J]. Materials Science and Engineering A, 2003, 263:140−151.
[25] LIU C L, AZIZI-ALIZAMINI H, PARSON N C, POOLE W J. The effect of Mn on microstructure evolution during homogenization of Al−Mg−Si−Mn alloys [J]. Materials Science Forum, 2014, 794−796: 1199−1204.
[26] GANESAN M, DYE D, LEE P D. A technique for characterizing microsegregation in multicomponent alloys and its application to single-crystal superalloy castings [J]. Metallurgical and Materials Transactions A, 2005, 36: 2191−2204.
[27] LOK Z J. Microchemistry in aluminium sheet production [D]. Delft: Delft University of Technology, 2005.

Al−Mg−Si−Mn−Fe 系合金均匀化过程中的显微组织演化：数值模拟与实验结果对比

C. L. LIU[1], H. AZIZI-ALIZAMINI[2], N. C. PARSON[3], W. J. POOLE[1], Q. DU[4]

1. Department of Materials Engineering, The University of British Columbia, Vancouver V6T 1Z4, Canada;
2. Department of Materials Science and Engineering, McMaster University, Hamilton L8S 4L7, Canada;
3. Rio Tinto, Arvida Research and Development Centre, P. O. Box 1250, Jonquière (QC) G7S 4K8, Canada;
4. SINTEF Materials and Chemistry, P. O. Box 4760 Sluppen, 7456 Trondheim, Norway

摘　要：通过数值模拟和实验相结合的方法，对 Al−Mg−Si−Mn−Fe (AA6xxx)系合金均匀化过程中的显微组织演化进行研究。所应用的数学模型是结合 CALPHAD 及基于 AA3xxx(Al−Mn−Fe−Si)系合金均匀化热处理而开发的。而后对此模型进行修正，以使得其应用拓展到更为复杂的 AA6xxx 系合金。该热处理模型可以预测包括溶质元素分布、初生相类型与比例、以及弥散相密度和尺寸分布在内的关键显微组织的演化。实验方面，对 3 种不同锰含量的 AA6xxx 系合金进行均匀化热处理。应用扫描电子显微镜、EPMA、XRD 和电阻率等实验手段对所得均匀化组织进行多角度表征。预测结果与实验表征的对比表明，数学模型可以较为准确地反映均匀化过程中显微组织的演化。

关键词：AA6xxx 合金；均匀化热处理；数学模型；CALPHAD； 扩散

(Edited by Wei-ping CHEN)